The effect of large-scale shear-velocity heterogeneity on SS precursor amplitudes

L. Bai[1] and J. Ritsema[2]

Received 11 November 2013; accepted 18 November 2013; published 5 December 2013.

[1] Precursors to the SS wave have been analyzed extensively to characterize seismic discontinuities in the upper mantle. We examine the influence of shear-velocity heterogeneity on the amplitude of underside shear wave reflections off the 410 (i.e., S410S) and 660 (i.e., S660S) discontinuities using waveform data from global seismic networks and spectral element method synthetics for four tomographic models of the crust and mantle. On average, the S660S/SS amplitude ratio is smaller than values predicted for the Preliminary Reference Earth Model (PREM) and tomographic models of shear velocity perturbations from PREM. The variation of S410S/SS and S660S/SS ratios determined for the 3-D models is significant. Its amplitude depends on the amplitude of shear-velocty heterogeneity in the mantle and on the incorporated model for the crust. The S410S/SS and S660S/SS amplitude variations are stronger in the data and do not correlate spatially with the simulated ratios. It is therefore not certain that the spatial variation of S410S/SS and S660S/SS, as expressed by cap averaging, can be related to compositional heterogeneity in the mantle, given the profound influence of the heterogeneous crust and mantle. **Citation:** Bai, L., and J. Ritsema (2013), The effect of large-scale shear-velocity heterogeneity on SS precursor amplitudes, *Geophys. Res. Lett.*, *40*, 6054–6058, doi:10.1002/2013GL058669.

1. Introduction

[2] Seismic discontinuities near 410 km and 660 km depths in the mantle (from hereon abbreviated as the 410 and 660) are due to pressure-induced mineral phase changes [e.g., *Ringwood*, 1991; *Frost*, 2008]. Constraints on 410 and 660 topography and impedance contrasts inform us of the thermal and compositional structure of the upper mantle and mass and heat transfer through the transition zone [e.g., *Bina and Helffrich*, 1994; *Helffrich*, 2000]. Observations of underside wave reflections off the 410 and the 660 (i.e., the SS precursors S410S and S660S and the PP precursors P410P and P660P) are often used to image the 410 and 660 on global [e.g., *Shearer*, 1991; *Gu et al.*, 1998; *Houser et al.*, 2008] and regional [e.g., *Rost and Weber*, 2002; *Schmerr and Garnero*, 2006; *Gu et al.*, 2009; *Heit et al.*, 2010; *Gu et al.*, 2012] scales. See *Deuss* [2009] for a review.

[3] Most studies have focused on estimating precursor travel times and the depths of the 410 and 660. Analyses of precursor amplitudes have addressed the relatively small P660P amplitude [e.g., *Estabrook and Kind*, 1996; *Shearer and Flanagan*, 1999], which suggests that the contrast in bulk modulus across the 660 is smaller than in standard seismic models. *Deuss and Woodhouse* [2001] and *Deuss et al*. [2006] have argued that multiple peaks in stacks of SS and PP precursors are due to phase transitions in both the olivine and garnet components of upper mantle rock. Lateral variations of precursor amplitudes have been attributed to melt, water, and other compositional heterogeneity in the upper mantle [e.g., *Chambers et al.*, 2005; *Lawrence and Shearer*, 2006; *Schmerr and Garnero*, 2007].

[4] Although amplitudes of SS precursors provide important constraints, it remains uncertain whether they can be interpreted robustly. *Shearer* [1993] speculated that wave focusing may obscure a correlation between precursor travel times and amplitudes. Velocity heterogeneity and crustal structure perturb body wave amplitudes [e.g., *Ritsema et al.*, 2002; *Tibuleac et al.*, 2003] and complicate precursor waveforms [*Zheng and Romanowicz*, 2012]. To investigate the effects of seismic heterogeneity in the crust and mantle on precursor amplitudes, we apply waveform stacking procedures to global seismic network data and synthetic seismograms for long-wavelength models of crust and mantle heterogeneity. This study extends the analysis by *Bai et al.* [2012] who examined the influence of mantle heterogeneity on precursor travel times. The available computational facilities limits us to analyzing spectral element method (SEM) [*Komatitsch and Tromp*, 2002] waveforms at periods longer than 16 s. Since PP precursors are not well separated at these relatively low frequencies, we analyze SS waveforms only.

2. Data and Processing

[5] We compute hour long transform-component SEM seismograms for models Preliminary Reference Earth Model (PREM) [*Dziewonski and Anderson*, 1981], PREMc, T1, T2, and T3. T1, T2, and T3 (Figure 1) are based on PREM's layered velocity structure. The depths of the 410 (at 400 km) and 660 (at 670 km) and the crustal structure are the same as in PREM. PREM's radial velocity structure in the mantle has been replaced by the tomographically derived shear velocities. Model T2 has the same structure as S20RTS. Models T1 and T3 are versions of S20RTS based on different damping parameters [*Ritsema et al.*, 2007]. Shear-velocity variations

[1]Key Laboratory of Continental Collision and Plateau Uplift, Institute of Tibetan Plateau Research, Chinese Academy of Sciences, Beijing, China.
[2]Department of Earth and Environmental Sciences, University of Michigan, Ann Arbor, Michigan, USA.

Corresponding author: L. Bai, Key Laboratory of Continental Collision and Plateau Uplift, Institute of Tibetan Plateau Research, Chinese Academy of Sciences, Beijing 100101, China. (bailing@itpcas.ac.cn)

0094-8276/13/10.1002/2013GL058669

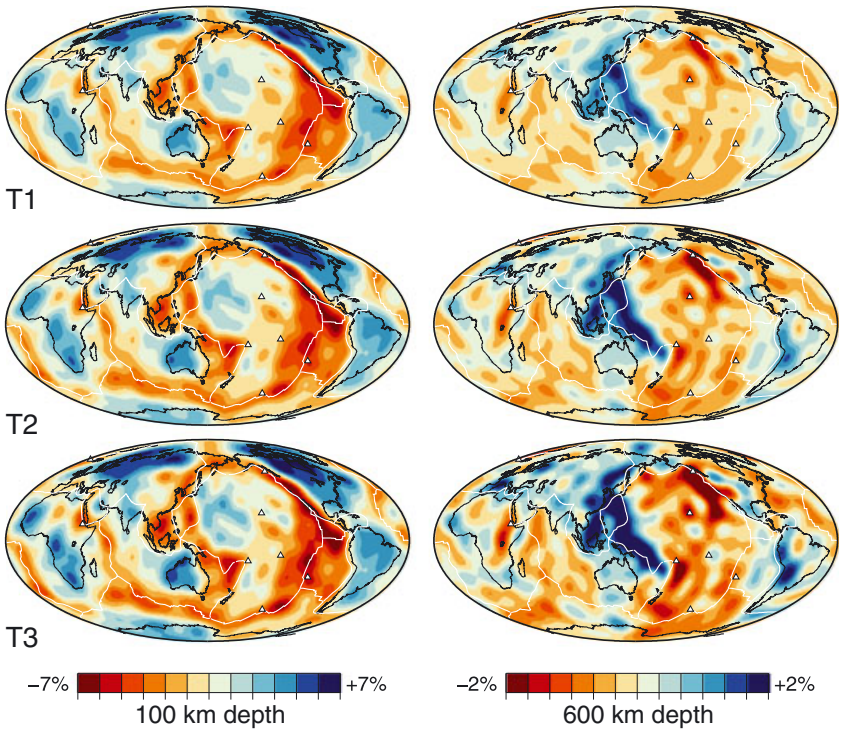

Figure 1. Maps of shear-velocity perturbations from PREM in models (top) T1, (middle) T2, and (bottom) T3 at depths of 100 km and 600 km. Note the different scales used to depict the variations.

in T1 are smoother and weaker than in S20RTS and stronger than S20RTS in model T3. T1 and T3 represent end-member models of the resolved spectra of shear-velocity heterogeneity in the most recently derived global models. Model PREMc has the same mantle structure as PREM. However, it has the inhomogeneous crustal structure of model Crust2.0 [*Bassin et al.*, 2000].

[6] The waveforms are computed for 34 earthquakes and 16,020 seismic stations. The earthquakes are at a depth of 20 km and have a dip-slip mechanism with strong teleseismic SS wave radiation. The seismic stations are on a global grid with 2° × 2° spacing. The density of SS bounce points is over 700 per 10° × 10°, and epicentral distances are uniformly sampled for subsets of waveforms with different SS bounce points.

[7] Our data set is the same as used by *Ritsema et al.* [2009]. It is derived from Incorporated Research Institutions for Seismology (IRIS) and Geoscope recordings of shallow (< 50 km) earthquakes between 1985 and 2007 with magnitudes between 6.0 and 7.4 at epicentral distances between 110° to 170°. The horizontal channels have been corrected for receiver response and rotated into radial and transverse components. We analyze SS precursors using the 25,000 transverse-component records with signal-to-noise ratios higher than 3. The waveforms have been band-pass filtered using a cosine square filter with cutoff frequencies of 4 mHz and 50 mHz and corner frequencies of 8 mHz and 40 mHz. They have been normalized so that all SS signals have positive polarities and amplitudes equal to 1.

[8] We align the waveforms on the SS arrival and sum subsets of traces with the same epicentral distances or with common SS surface reflection points to raise the SS precursors above the noise. We account for slowness differences between SS and the precursors using the PREM model. The amplitude ratios of SS and S410S (S410S/SS) and of SS and S660S (S660S/SS) are computed by cross correlation following *Ritsema and van Heijst* [2002].

[9] Figure 2 shows representative stacks of the S410S and S660S signals recorded in data and simulated for PREM, T1, T2, T3, and PREMc. In this case, the summed waveforms have common SS reflection points in the Mozambique Channel. The misalignment of S410S and S660S and the variable S410S/SS and S660S/SS amplitude ratios are due to differences in the real and modeled shear-velocity structure of the mantle.

3. Results

3.1. Epicentral Distance Variation

[10] Figures 3a and 3b show S410S/SS and S660S/SS as a function of epicentral distance. The measurements have been averaged in 5° wide overlapping distance bins. S410S/SS and S660S/SS increase smoothly because the S410S and S660S reflection coefficients increase with increasing distance. Large departures from the general trends for S410S/SS near 140° and for S660S/SS near 115° are due to the interference of S410S and S660S with ScS660ScS and S_{diff}s660s (Figure 3c), respectively. The waveforms near these distances are excluded from the analysis.

[11] The S410S/SS amplitude ratio determined for PREM and T2 is slightly higher than the recorded amplitude ratios, especially for the 110°–125° distance range. However, the S660S/SS amplitude ratio for PREM and T2 is 2 to 3 times higher than the recorded amplitude ratio (see also Figure 2), in agreement with previous observations by *Shearer and Flanagan* [1999].

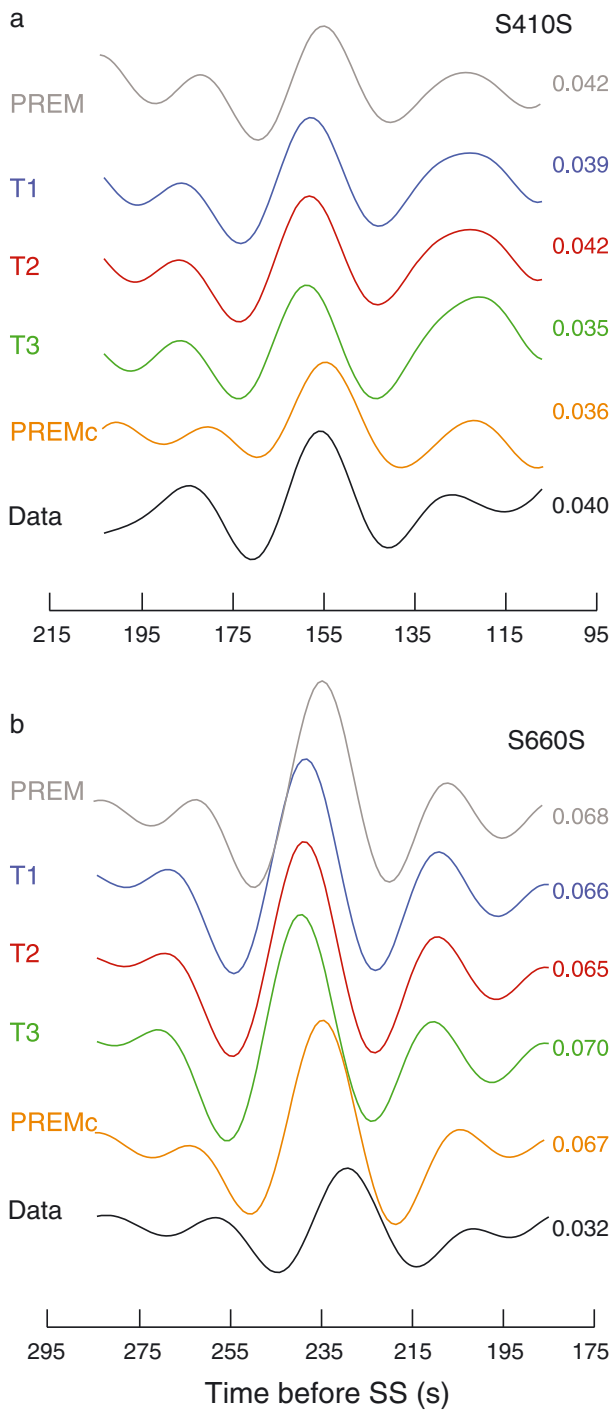

Figure 2. Stacks of computed waveforms of (a) S410S and (b) S660S for (from top to bottom in each panel) models PREM, T1, T2, T3, PREMc, and for the data (bottom trace). The S410S/SS and S660S/SS amplitude ratios are indicated on the right. The stacked traces have SS surface reflection points in a circle with a radius of 15° centered at (20°S, 40°E) in the Mozambique Channel. The expected arrival times of S410S (= 155.0 s) and S660S (= 235.1 s) before SS are determined for an epicentral distance of 135°.

3.2. Geographical Variations

[12] Figure 4 shows the lateral variations of S410S/SS and S660S/SS amplitude ratios. These are estimated from stacks determined by summing waveforms with SS surface reflection points that fall in a circle with a radius of 15°. The amplitude ratios are plotted at the center of these circular caps. We have subtracted the average values of S410S/SS and S660S/SS to emphasize their spatial variation and we have corrected for the quasi-linear increase of S660S/SS with epicentral distance using the PREM simulations. This correction is fairly minor because the distribution of the epicentral distances is similar for all bounce points.

[13] The cap radius of 15° is larger than the more typical 10° cap used in SS precursor analysis. However, significant differences between the stacks of data and the stacks of synthetics stand out despite stronger smoothing. The amplitude variations for the PREM model are smaller than the variations resolved for the 3-D models and the data. Thus, the spatial variations S410S/SS and S660S/SS resolved in the data and in T1, T2, T3, and PREMc are not artifacts of processing.

[14] The variation in the recorded S410S/SS and S660S/SS ratios is about 3 times stronger than the ratios determined for T1, T2, and T3. The synthetic ratios are slightly stronger for model T3 (the tomographic model based on weakest norm damping). In addition, the variations in S410S/SS and S660S/SS for model T3 are different, notably in Pacific.

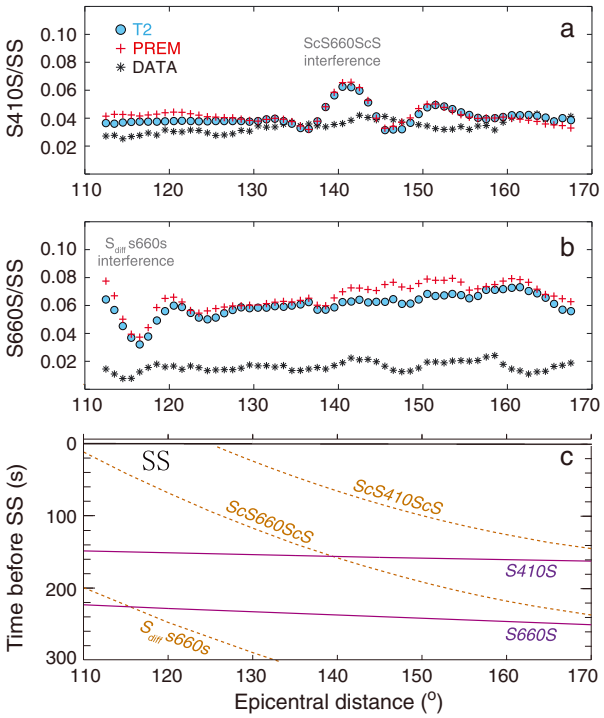

Figure 3. Amplitude ratios of (a) S410S/SS and (b) S660S/SS measured in stacks of waveform data (stars) and SEM waveforms computed for models T2 (blue circles) and PREM (red crosses). Data are averaged within ±2.5° wide epicentral distance bins. (c) Ray theoretical travel times. These include SS (black line); the SS precursors S410S and S660S (purple); and the ScS2 precursors ScS410ScS and ScS660ScS and the phase S_{diff} s660s (brown).

[15] For model PREMc, which is identical to PREM except for the included Crust2.0 crustal structure, the patterns in S410S/SS and S660S/SS are different than for T1, T2, and T3. S660S/SS, in particular, is clearly high for SS bounce points beneath Eurasia and low for Pacific bounce points. This is contrary to the variations seen for 3-D mantle models even though they include the same crustal structure as PREMc. Hence, the long-wavelength shear-velocity variations in the mantle have an effect on S410S/SS and S660S/SS that is as strong as the influence of the crust.

[16] To illustrate the variable range of amplitude ratios, we compare in Figure 5 histograms of the absolute values

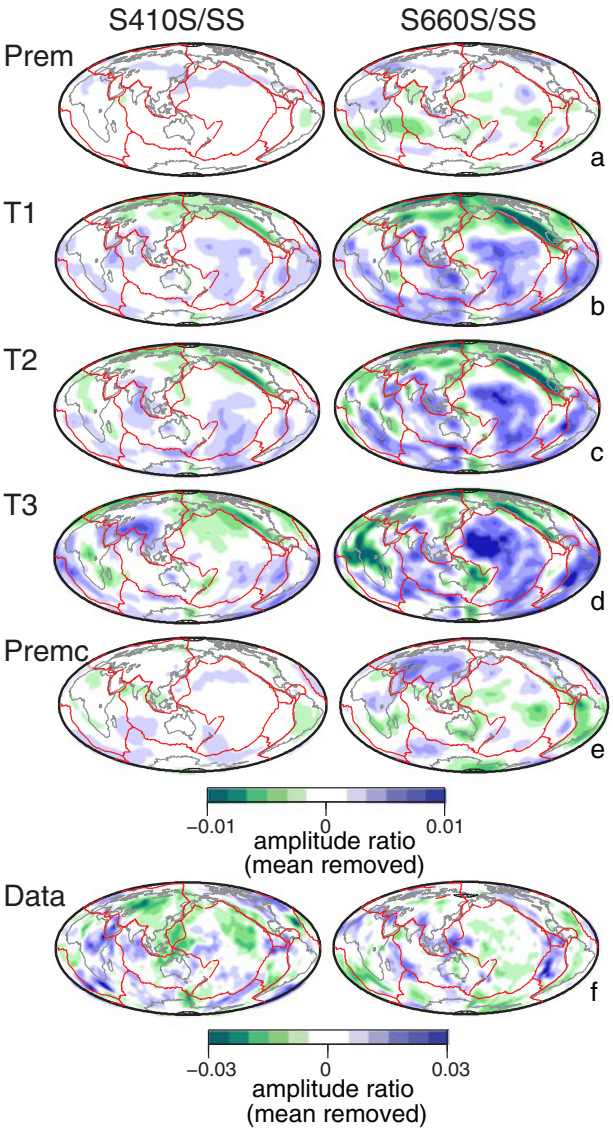

Figure 4. Lateral variation of (left) S410S/SS and (right) S660S/SS determined for models (a) PREM, (b) T1, (c) T2, (d) T3, (e) PREMc, and determined using (f) waveform data. The values are plotted at the SS surface reflection points. They are determined using a stack of waveforms corresponding to source-receiver pairs with SS reflection points that fall within a circle with a radius of 15°. The mean value has been subtracted. For the 12 colors used to plot the amplitude ratios, the data values range from –0.03 to +0.03 and the values for the SEM stacks range from –0.01 to +0.01.

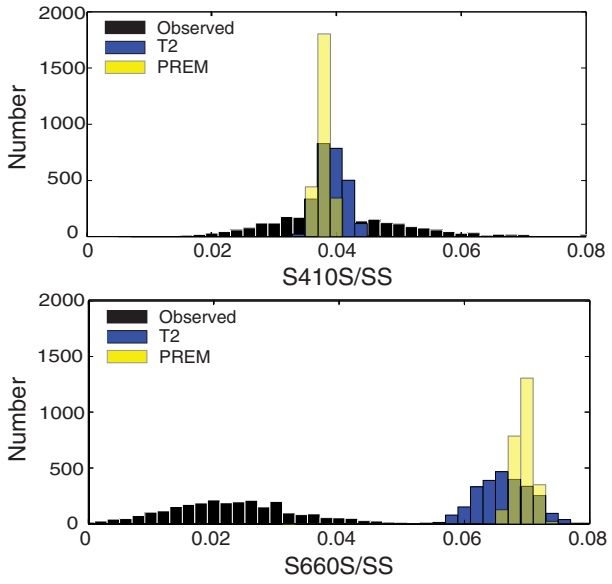

Figure 5. Histograms of the cap-averaged values of (top) S410S/SS and (bottom) S660S/SS from Figure 4 for the data (black), model T2 (blue), and model PREM (yellow).

of S410S/SS and S660S/SS recorded in stacks of data and in stacks of SEM waveforms for models T2 and PREM. On average, the simulated S410S/SS and S660S/SS amplitudes range between 0.038 ± 0.005 and 0.064 ± 0.008. The recorded S410S/SS and S660S/SS amplitude ratios are about 0.041 ± 0.029, and 0.024 ± 0.024.

[17] In agreement with previous studies [e.g., *Shearer and Flanagan*, 1999; *Lawrence and Shearer*, 2006; *Deuss*, 2009], the observed S660S/SS amplitude ratios are smaller than the simulated ratios by about a factor of 3 (Figure 3). On average, S660S/SS ratio is 6.5% for model T2 and 3.2% for the data. The spread (95% of the values) in S410S/SS and S660S/SS for the recordings is 0.012–0.070 and 0–0.048, and for model T2 is 0.035–0.043 and 0.057–0.076 (Figure 5).

4. Discussion and Conclusions

[18] S410S/SS and S660S/SS are strongest for T3, the model with the strongest shear-velocity heterogeneity. The large-scale patterns in the S410S/SS and S660S/SS amplitude ratios (Figures 4b–4d) for T1, T2, and T3 do not correlate with the ratios determined for the waveform data nor do they correlate with the shear-velocity heterogeneity of these models (Figure 1). This is in agreement with *Shearer* [1993], who did not observe a correlation between precursor travel time and amplitude anomalies. Thus, the contribution of shear-velocity heterogeneity to S410S/SS and S660S/SS is not limited to the SS bounce point region.

[19] We measure a robust variation in the S410S/SS and S660S/SS amplitude ratio with patterns and magnitudes similar to what had been resolved by *Chambers et al.* [2005] and *Shearer* [1993]. It is possible that the S410S/SS and S660S/SS data include a signal of variable impedance contrasts across the 410 and 660. However, the measurements of these amplitude ratios using SEM waveforms demonstrate that long-wavelength shear-velocity heterogeneity in the mantle is responsible for a significant portion

of this signal. Although the simulated amplitude ratios are smaller than the observed ratios, it is likely that they underestimate the effects of wave focusing as horizontal wave speed gradients are reduced by damping in the tomographic inversion. It is therefore not clear that lateral variations in S410S/SS and S660S/SS can be related to compositional heterogeneity in the upper mantle.

[20] **Acknowledgments.** This research is funded by the grants of National Nature Science Foundation of China (41274086) and of National Science Foundation of U.S. (EAR-1015172). Waveform data have been provided by IRIS and Geoscope. The GMT software [*Wessel and Smith*, 1995] has been used to make figures.

[21] The Editor thanks Arwen Deuss and an anonymous reviewer for their assistance in evaluating this paper.

References

Bai, L., Y. Zhang, and J. Ritsema (2012), An analysis of SS precursors using 3D spectral-element method seismograms, *Geophys. J. Int.*, *188*, 293–300, doi:10.1111/j.1365-246X.2011.05256.x.

Bassin, C., G. Laske, and G. Masters (2000), The current limits of resolution for surface wave tomography in North America, *EOS Trans. AGU, 81*(48), Fall Meet. Suppl., Abstract S12A-03.

Bina, C. R., and G. Helffrich (1994), Phase transition Clapeyron slopes and transition zone seismic discontinuity topography, *J. Geophys. Res.*, *99*, 15,853–15,860.

Chambers, K., A. Deuss, and J. H. Woodhouse (2005), Reflectivity of the 410-km discontinuity from PP and SS precursors, *J. Geophys. Res.*, *110*, B02301, doi:10.1029/2005JB003345.

Deuss, A. (2009), Global observations of mantle discontinuities using SS and PP precursors, *Surv. Geophys.*, *30*, 301–326.

Deuss, A., and J. H. Woodhouse (2001), Seismic observations of splitting of the mid-transition zone discontinuity in Earth's mantle, *Science*, *294*, 354–357.

Deuss, A., S. A. T. Redfern, K. Chambers, and J. H. Woodhouse (2006), The nature of the 660-kilometer discontinuity in Earth's mantle from global seismic observations of PP precursors, *Science*, *311*, 198–201, doi:10.1126/science.1120020.

Dziewonski, A. M., and D. L. Anderson (1981), Preliminary reference Earth model, *Phys. Earth Planet. Int.*, *25*, 297–356.

Estabrook, C. H., and R. Kind (1996), The nature of the 660-kilometer upper-mantle seismic discontinuity from precursors to the PP phase, *Science*, *274*, 1179–1182.

Frost, D. (2008), The upper mantle and transition zone, *Elements*, *4*, 171–176, doi:10.2113/GSELEMENTS.4.3.171.

Gu, Y. J., A. M. Dziewonski, and C. B. Agee (1998), Global de-correlation of the topography of transition zone discontinuities, *Earth Planet. Sci. Lett.*, *157*, 57–67.

Gu, Y. J., Y. An, M. Sacchi, R. Schultz, and J. Ritsema (2009), Mantle reflectivity structure beneath oceanic hotspots, *Geophys. J. Int.*, *178*, 1456–1472.

Gu, Y. J., A. Okeler, and R. Schultz (2012), Tracing slabs beneath northwestern pacific subduction zones, *Phys. Earth Planet. Int.*, *331-332*, 269–280, doi:10.1016/j.epsl.2012.03.023.

Heit, B., X. Yuan, M. Bianchi, R. Kind, and J. Gossler (2010), Study of the lithospheric and upper-mantle discontinuities beneath eastern Asia by SS precursors, *Geophys. J. Int.*, *183*, 252–266.

Helffrich, G. R. (2000), Topography of the transition zone discontinuities, *Rev. Geophys.*, *38*, 141–158.

Houser, C., G. Masters, M. Flanagan, and P. M. Shearer (2008), Determination and analysis of long-wavelength transition zone structure using SS precursors, *Geophys. J. Int.*, *174*, 178–194.

Komatitsch, D., and J. Tromp (2002), Spectral-element simulations of global seismic wave propagation—I. Validation, *Geophys. J. Int.*, *149*, 390–412.

Lawrence, J. F., and P. M. Shearer (2006), Constraining seismic velocity and density for the mantle transition zone with reflected and transmitted waveforms, *Geochem. Geophys. Geosyst*, *7*, Q10012, doi:10.1029/2006GC001339.

Ringwood, A. E. (1991), Phase transformations and their bearing on the constitution and dynamics of the mantle, *Geochim. Cosmochim. Acta*, *55*, 2083–2110.

Ritsema, J., and H. J. van Heijst (2002), Constraints on the correlation of P- and S-wave velocity heterogeneity in the mantle from P, PP, PPP, and PKPab traveltimes, *Geophys. J. Int.*, *149*, 482–489.

Ritsema, J., L. A. Rivera, D. Komatitsch, J. Tromp, and H. J. van Heijst (2002), Effects of crust and mantle heterogeneity on PP/P and SS/S amplitude ratios, *Geophys. Res. Lett.*, *29*, 1430, doi:10.1029/2001GL013831.

Ritsema, J., A. K. McNamara, and A. Bull (2007), Tomographic filtering of geodynamic models: Implications for model interpretation and large-scale mantle structure, *J. Geophys. Res.*, *112*, B01303, doi:10.1029/2006JB004566.

Ritsema, J., W. Xu, L. Stixrude, and C. Lithgow-Bertelloni (2009), Estimates of the transition zone temperature in a mechanically mixed upper mantle, *Earth Planet. Sci. Lett.*, *277*, 244–252, doi:10.1029/2003JB002610.

Rost, S., and M. Weber (2002), The upper mantle transition zone discontinuities in the Pacific as determined by short-period array data, *Earth Planet. Sci. Let.*, *204*, 347–361.

Schmerr, N., and E. J. Garnero (2006), Investigation of upper mantle discontinuity structure beneath the central pacific using SS precurfors, *J. Geophys. Res.*, *111*, B08305, doi:10.1029/2005JB04197.

Schmerr, N., and E. J. Garnero (2007), Upper mantle discontinuity topography from thermal and chemical heterogeneity, *Science*, *318*, 623–626.

Shearer, P. M. (1991), Constraints on upper-mantle discontinuities from observations of long-period reflected and converted phases, *J. Geophys. Res.*, *96*, 18,147–18,182.

Shearer, P. M. (1993), Global mapping of upper mantle reflectors from long-period SS precursors, *Geophys. J. Int.*, *115*, 878–904.

Shearer, P. M., and M. Flanagan (1999), Seismic velocity and density jumps across the 410- and 660-kilometer discontinuities, *Science*, *285*, 1545–1548.

Tibuleac, I. M., G. Nolet, C. Michaelson, and I. Koulakov (2003), P wave amplitudes in a 3D earth, *Geophys. J. Int.*, *155*, 1–10, doi:10.1046/j.1365-246X.2003.01969.x.

Wessel, P., and W. H. F. Smith (1995), New version of the generic mapping tools released, *EOS Trans. AGU*, *76*(33), 329, doi:10.1029/95EO00198.

Zheng, Z., and B. Romanowicz (2012), Do double SS precursors mean double discontinuities?, *Geophys. J. Int.*, *191*, 1361–1373, doi:10.1111/j.1365-246X.2012.05683.x.